ORIGINAL CONTRIBUTION

Determination of axial forces during the capillary breakup of liquid filaments – the tilted CaBER method

**Dirk Sachsenheimer · Bernhard Hochstein ·
Hans Buggisch · Norbert Willenbacher**

Abstract The capillary breakup extensional rheometry (CaBER) is a versatile method to characterize the elongational behavior of low-viscosity fluids. Commonly, data evaluation is based on the assumption of zero normal stress in axial direction ($\sigma_{zz} = 0$). In this paper, we present a simple method to determine the axial force using a CaBER device rotated by 90° and analyzing the deflection of the filament due to gravity. Forces in the range of 0.1–1,000 μN could be assessed. Our study includes experimental investigations of Newtonian fructose solutions and silicon oil mixtures (viscosity range, 0.9–60 Pa s) and weakly viscoelastic polyethylene oxide (PEO, $M_w = 10^6$ g/mol) solutions covering a concentration range from $c \approx c*$ (critical overlap concentration) up to $c > c_e$ (entanglement concentration). Papageorgiou's solution for the stress ratio σ_{zz}/σ_{rr} in Newtonian fluids during capillary thinning is experimentally confirmed, but the widely accepted assumption of vanishing axial stress in weakly viscoelastic fluids is not fulfilled for PEO solutions, if c_e is exceeded.

Keywords CaBER · Elongational viscosity · Uniaxial extension · Force measurement

D. Sachsenheimer (✉) · B. Hochstein ·
H. Buggisch · N. Willenbacher
Karlsruhe Institute of Technology (KIT),
Institute for Mechanical Process Engineering
and Mechanics, Group Applied Mechanics (AME),
Gotthard-Franz-Straße 3, 76131 Karlsruhe, Germany
e-mail: sachsenheimer@kit.edu

Introduction

General remarks

Many industrial applications and processes such as coating (Fernando et al. 1989, 2000), spraying (Dexter 1996; Prud'homme et al. 2005) (including mist formation (James et al. 2003) and its prevention (Chao et al. 1984)), inkjet printing (Agarwal and Gupta 2002; Han et al. 2004; Vadillo et al. 2010) or fiber spinning (McKay et al. 1978) include flow kinematics with large elements of elongational flow. Due to this high technical relevance, the correlation between rheological properties against elongational deformation and fluid behavior in processes is a major subject of research.

Technically relevant liquids are often complex multi-component systems with special flow properties adjusted by adding small amounts of rheological modifier or thickener. A great number of these additional materials are commercially available, e.g., biopolymers (polysaccharides) like xanthan gum, starch, carrageenan, or especially cellulose derivatives, inorganic substances like silica or water-swellable clay, or simply synthetic polymers like polyacrylates, polyvinylpyrilidone, or polyethylene oxide (PEO) (Braun and Rosen 2000). Therefore, understanding the elongational flow properties of such viscoelastic polymer solutions is of fundamental importance in process optimization and product development. Unfortunately, measuring the elongational viscosity of low viscosity fluids is still a very challenging task, resulting in only a few investigations which correlate the elongational behavior of complex fluids with their application properties (Meadows et al. 1995; Kennedy et al. 1995; Ng et al. 1996; Solomon

and Muller 1996; Tan et al. 2000; Stelter et al. 2002; Plog et al. 2005).

Nevertheless, a simple and versatile method for the characterization of low-viscosity fluids has been suggested more than 20 years ago (Bazilevsky et al. 1990; Entov and Hinch 1997; Bazilevsky et al. 2001), this so called capillary breakup extensional rheometer (CaBER) is even commercially available now. In this experiment, an instable liquid filament is created by applying a step strain, and the diameter of this liquid bridge is monitored as a function of time. In contrast to other techniques, CaBER allows for large Hencky strains which are of great significance to industrial practice. Unfortunately, evaluating the elongational viscosity is not trivial for CaBER experiments since no axial force is measured. Accordingly, apparent elongational viscosities are often calculated for CaBER.

In this paper, we introduce the tilted CaBER method as a simple and accurate way to determine the axial force $F(t)$ and the elongational rate $\dot{\varepsilon}$ during filament thinning at the same time by only analyzing video images. The conventional CaBER device is rotated by 90°, and the bending of the liquid filament due to gravity is recorded using a high-speed camera. First, we describe the principles of calculating the (apparent) elongational viscosity from CaBER measurements and discuss the typical decrease of the diameter for Newtonian and viscoelastic fluids. Then, we describe how to calculate the force from the deflection of a fluid filament. After this, we present the experimental setup and give a short overview of the samples used, including preparation and characterization. Following with the experimental part, we verify the tilted CaBER method using Newtonian fluids and apply it to non-Newtonian PEO solutions. Finally, concluding remarks are given.

Force balance for a straight vertical cylindrical thread

The axial force F in a cylindrical filament with axial orientation into the direction of gravity (here, z-direction) is assumed to be independent of the z-position, but F may depend on time. Taking into account the surface tension Γ, the normal stresses σ_{zz} and σ_{rr}, but neglecting gravity and inertia effects (see Fig. 1), the total force balances in z-direction reads as follows:

$$\frac{\pi}{4}\sigma_{zz}D^2 + \pi\Gamma D = F \Rightarrow \sigma_{zz} = \frac{4\left(F - \pi\Gamma D\right)}{\pi D^2}. \quad (1)$$

McKinley and Tripathi (2000) used the ratio X between the true axial force F in the filament and the value resulting from the assumption $\sigma_{zz} = 0$ in order to
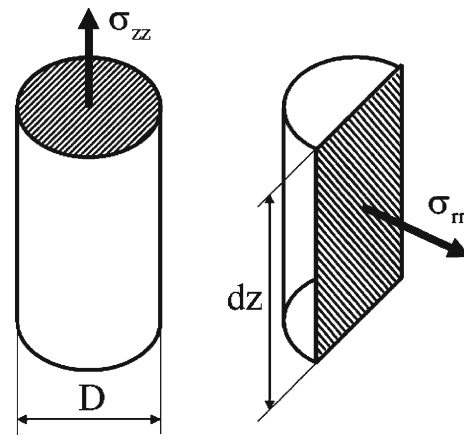

Fig. 1 Cut filament (*hatched areas*) with normal stresses σ_{zz} and σ_{rr}

quantify the influence of the axial normal stress σ_{zz}.

$$X = \frac{F}{F_{\sigma_{zz}=0}} = \frac{F}{\pi\Gamma D} \quad (2)$$

For an infinitesimal volume element with length dz and diameter D, the force balance in r-direction reads as follows:

$$\sigma_{rr}D\,dz + 2\Gamma\,dz = 0 \Rightarrow \sigma_{rr} = -\frac{2\Gamma}{D}. \quad (3)$$

Calculation of the elongational viscosity

The elongational viscosity η_e for uniaxial elongational flows like, e.g., in CaBER experiments is given by Schümmer and Tebel (1983):

$$\eta_e = \frac{\sigma_{zz} - \sigma_{rr}}{\dot{\varepsilon}}. \quad (4)$$

Insertion of the axial normal stress σ_{zz} (Eq. 1) and the radial normal stress σ_{rr} (Eq. 3) into Eq. 4 results in the following expression for the true elongational viscosity valid for cylindrical or at least slender filaments:

$$\eta_e = \frac{4F - 2\pi\Gamma D}{\pi D^2\dot{\varepsilon}}. \quad (5)$$

Using the definition of the elongation rate

$$\dot{\varepsilon} = -\frac{2}{D}\frac{dD}{dt}, \quad (6)$$

equation 5 yields

$$\eta_e = \frac{\Gamma}{dD/dt} - \frac{2F}{\pi D\,dD/dt}. \quad (7)$$

For the sake of completeness, expressions for the radial normal stress and the elongational viscosity in case of non-cylindrical filaments are given in Appendix.

It is obvious from Eq. 7 that for calculating η_e, the diameter D and the force F are needed. Therefore, CaBER experiments with simultaneous force measurements allow for the determination of the true elongational viscosity for any fluid without assumption of special constitutive equations.

But the evaluation of Eq. 7 is not trivial for CaBER experiments since no axial force measurement is included, and, hence, the normal stress σ_{zz} is not known. Instead, η_e is often evaluated using the assumption $\sigma_{zz} = 0$. Then an apparent elongational viscosity for CaBER experiments is obtained (Anna and McKinley 2001):

$$\eta_{e,app} = -\frac{\Gamma}{dD/dt}. \tag{8}$$

So far, the $\sigma_{zz} = 0$ assumption has not been validated experimentally for the CaBER experiment. Deviations obviously occur for the Newtonian case (Liang and Mackley 1994; Kolte and Szabo 1999; McKinley and Tripathi 2000) and also shown in numerical simulations of the CaBER experiment using different viscoelastic or viscoplastic constitutive equations (Clasen et al. 2006a; Webster et al. 2008; Alexandrou et al. 2009).

Therefore, fluid characterization based on Eq. 8 might be helpful in comparative studies employed, e.g., for product development purposes. But especially for the determination of the true elongational viscosity from CaBER experiments, it is mandatory to measure the time-dependent axial force F during filament thinning accurately. The magnitude of this force can be roughly estimated from the force balance in axial direction (Eq. 1) using the $\sigma_{zz} = 0$ assumption. Typically, Γ is in the range of 20–70 mN/m, and the filament diameter decays from 1 mm to about 10 μm. This corresponds to a force range 0.5 μN $< F(t) <$ 220 μN. The first attempt to implement a force transducer into a CaBER device was done by Klein et al. (2009). They mounted a commercial quartz load cell to the fixed bottom plate of their apparatus. Due to oversampling of the force signal, a nominal sensitivity of 50 μN was reached, but calibration was only done in the force range larger than 2,000 μN. Thus, reliable force detection during capillary thinning of fluid filaments was not possible.

Time evolution of the filament diameter for Newtonian and weakly viscoelastic fluids

The time evolution of the diameter during capillary thinning is controlled by a balance of capillary and viscous or viscoelastic forces. Different characteristic in diameter vs. time curves are observed for different types of fluids, e.g., Bingham plastic, power law, and Newtonian or viscoelastic fluids.

The midpoint diameter D_{mid} of a Newtonian fluid in a CaBER experiment decreases linearly with time t according to Papageorgiou (1995) and McKinley and Tripathi (2000):

$$D_{mid}(t) = D_1 - \Theta\frac{\Gamma}{\eta_s}t \tag{9}$$

where D_1 is the initial diameter of the liquid bridge at time $t = 0$ at which linear thinning of the filament sets in, Γ is the surface tension, Θ is a constant numerical factor, and η_s is the shear viscosity. The local force balance ($\sigma_{zz} = 0$) for a thinning liquid yields $\Theta = 0.333$ if only the surface tension is considered. Papageorgiou (1995) calculated the numerical factor to $\Theta = 0.1418$ in case of negligible inertia (Reynolds number Re $\rightarrow 0$). Considering inertia (Re > 0), Eggers (1993, 1997) and Brenner et al. (1996) estimated the numerical factor to $\Theta = 0.0608$ and showed that this solution is valid near the filament break up.

McKinley and Tripathi (2000) confirmed the numerical results of Papageorgiou (1995) ($\Theta = 0.1418$) experimentally using glycerol samples and related the factor Θ to the force ratio X (Eq. 2).

$$X = \frac{3\Theta + 1}{2} \tag{10}$$

The experimental validated $\Theta = 0.1418$ value corresponds to $X = 0.713$. This indicates that the axial force is not only given by the surface tension, and an additional axial normal stress must be present for Newtonian liquid filaments.

In contrast to Newtonian liquids, weakly elastic polymer solutions with concentrations $c < c_e$ form cylindrical filaments, and their diameter decreases exponentially with time in CaBER experiments (Bazilevsky et al. 1990; Entov and Hinch 1997; Anna and McKinley 2001; Arnolds et al. 2010).

$$D(t) = D_1\left(\frac{GD_1}{\Gamma}\right)^{1/3}\exp\left(-\frac{t}{3\lambda_e}\right) \tag{11}$$

where D_1 is the initial diameter of the filament at the beginning of the exponential decrease, G is the elastic modulus, and λ_e is the elongational relaxation time, which is related to the constant elongation rate $\dot{\varepsilon} = 2/(3\lambda_e)$ (see also Eq. 6).

Exponential thinning for viscoelastic fluids can also result if an exponentially increasing normal stress is assumed instead of $\sigma_{zz} = 0$ (Clasen et al. 2006a). Clasen et al. (2006a) stated that σ_{zz} increases with the same time constant as $D(t)$. Then Eq. 11 has to be corrected

by a factor of $4^{-1/3} \approx 0.63$, but the elongational relaxation time λ_e remains unaffected.

There is no simple universal relationship between this characteristic elongational relaxation time and shear relaxation time. For a series of PIB solutions, $\lambda_e \approx 3\bar{\lambda}_s$ was reported, with $\bar{\lambda}_s$ defined as an average shear relaxation time (Liang and Mackley 1994). For PS Boger fluids with concentrations $c \approx c*$, elongational relaxation times λ_e close to the Zimm relaxation time λ_Z were found (Bazilevskii et al. 1997); but on the other hand, it was clearly shown for PEO as well as PS solutions that λ_e can vary drastically even at $c < c*$ and λ_e/λ_Z values between 0.1 and 10 have been documented (Tirtaatmadja et al. 2006; Christanti and Walker 2001a, b; Clasen et al. 2006a, b). Oliveira et al. (2006) related λ_e to the longest relaxation time λ_s estimated from small amplitude oscillatory shear and found $\lambda_e \approx \lambda_s$ PEO solutions with $c \approx c*$. Arnolds et al. (2010) observed that $\lambda_e/\lambda_s \leq 1$ and strongly decreases with increasing c for PEO solutions with $c* < c < c_e$ and attributed this to the large deformation the solutions experience during filament thinning. They used a simple factorable integral model including a single relaxation time and a damping function to calculate λ_e/λ_s and obtained good agreement with experimental results.

Other more complex systems like surfactant solutions forming entangled wormlike micelles, polyelectrolyte complexes in solution or aggregated acrylic thickener solutions also exhibit relaxation time ratios $\lambda_e/\lambda_s < 1$, but these systems are supposed to undergo structural changes in strong elongational flow (Bhardwaj et al. 2007; Kheirandish et al. 2008; Willenbacher et al. 2008).

Finally, it should be mentioned that PEO solutions with $c > c_e$ still form cylindrical filaments, but the time evolution of the filament diameter is no longer exponential and cannot be characterized by a single relaxation time λ_e (Arnolds et al. 2010).

Determination of the axial force in a horizontally stretched filament

A fluid filament is bent when gravity is acting in radial direction and the axial force within the liquid can be calculated from the bending line. Figure 2 shows a section of a liquid filament with infinitesimal length, ds, and the acting gravity force, dF_G. The axial force is generally not constant, which is considered in the contribution of the infinitesimal force, dF, between the left and right edge of the pictured thread. In order to evaluate the axial force, all forces are balanced with
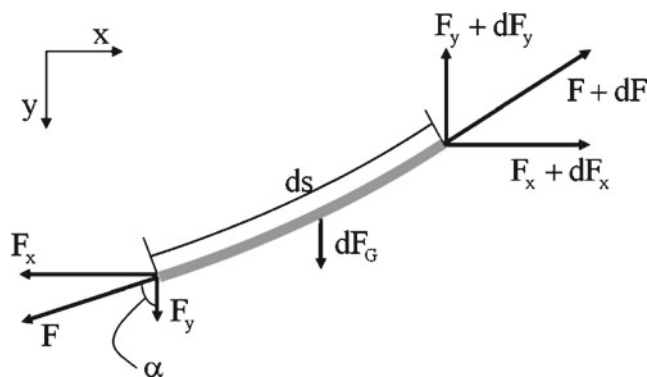

Fig. 2 Forces in a tilted liquid thread (*gray*) with infinitesimal length ds

respect to a (x, y) coordinate system fixed in space. Figure 3 presents the constructional realization of the tilted CaBER method and the bent liquid filament.

It is clearly shown in Fig. 2 that the force balances in x- and y-direction results in $dF_x = 0$ or $F_x = C_1$, where C_1 is a constant of integration and $dF_y = dF_G$. The gravity force is proportional to the volume dV and is calculated assuming constant diameter D and density ρ:

$$dF_G = g \, dm = \rho g \, dV = \frac{\pi}{4}\rho g D^2 \, ds. \qquad (12)$$
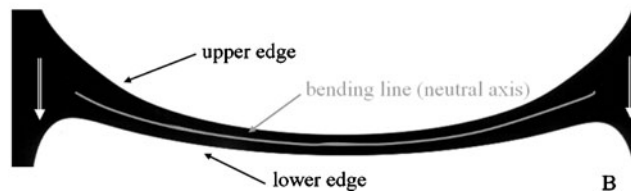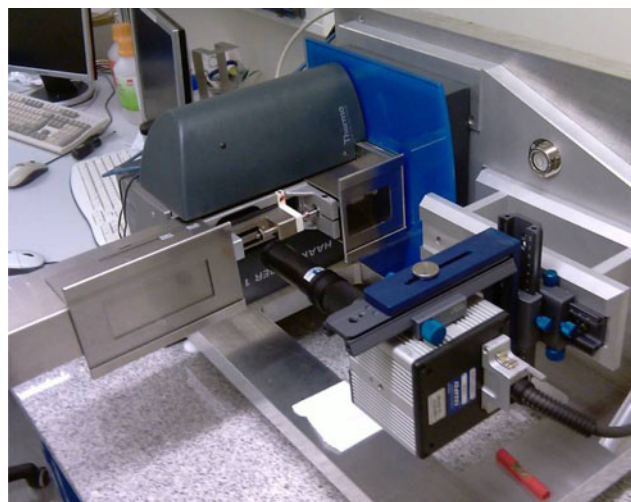
Fig. 3 a The constructional realization of the tilted CaBER method. **b** The bent liquid filament

Furthermore, ds can be written as

$$ds = \sqrt{(dx)^2 + (dy)^2} = dx \sqrt{1 + \left(\frac{dy}{dx}\right)^2} \tag{13}$$

and finally

$$\frac{dF_y}{dx} = \frac{dF_G}{dx} = \frac{\pi}{4} \rho g D^2 \sqrt{1 + (y')^2} \tag{14}$$

where y' is the first derivative of the bending line y with respect to x. The left side of Eq. 14 is obtained from the geometrical ratio

$$\frac{F_x}{F_y} = \frac{dx}{dy} \Rightarrow \frac{dF_y}{dx} = F_x \, y''. \tag{15}$$

Combining Eqs. 14 and 15 yields the differential equation for the bending line of the so called torque-free curved beam (see also Gross et al. 2009):

$$y'' = \frac{\pi \rho g D^2}{4 F_x} \sqrt{1 + (y')^2}. \tag{16}$$

We use the substitutions $y' = u$ and $y'' = u'$ to solve the differential Eq. 16, and we choose the position of maximum deflection as point of reference to calculate the constants of integration. Thus, we get the second derivative of the bending line y'' as a function of the x-position and the force component F_x:

$$y'' = \frac{\pi \rho g D^2}{4 F_x} \cosh\left(\frac{\pi \rho g D^2}{4 F_x} x\right). \tag{17}$$

The absolute value of the force F can be calculated as a function of F_x and x analogous to the approach taken in Eq. 13, using Eq. 15 and the identity $\cosh^2(\varphi) - \sinh^2(\varphi) = 1$.

$$F = F_x \cosh\left(\frac{\pi \rho g D^2}{4 F_x} x\right) \tag{18}$$

Equations 17 and 18 can be developed in Taylor series. Taking into account the first two terms (O(2)), the axial force F is no longer a function of the position x and is given by

$$F = \frac{\pi \rho g}{4 w''} D^2. \tag{19}$$

For sake of clarity, we use the symbol w for the approximated bending line and w'' for its second derivative.

The data evaluation is based on a least square approximation of the bending line by using a second order polynomial and calculating the constant second derivative w'' to be inserted in Eq. 19. However, a constant diameter is assumed so far. This disadvantage can be avoided using the deflection of the liquid thread instead of the curvature of the bending line. Then, integrating Eq. 19 twice yields the following relationship between the axial force and the diameter $D(t, x)$:

$$F = \frac{\pi \rho g}{4 w} \int_0^x \int_0^{\tilde{x}} D\left(\hat{x}\right)^2 d\hat{x} d\tilde{x}. \tag{20}$$

The double integral in Eq. 20 can be solved numerically without any fitting of the bending line or any other assumptions.

We estimate the approximation error, which may be defined as follows:

$$\beta = 1 - w/y \tag{21}$$

where y is the true and w the approximated bending line. For given F and D, F_x is calculated numerically in order to estimate the approximation error β. Lines of constant β are shown in Fig. 4 for a cylindrical fluid filament with density $\rho = 1$ g/cm^3 and length $2x = 12$ mm. For the experiments presented here, β was always below 0.1 %. It should be noted that the length of the filament has a drastic influence on the approximation error. For example, doubling the length of the filament to 24 mm while leaving the other parameters unchanged results in $1 \% < \beta < 10 \%$.
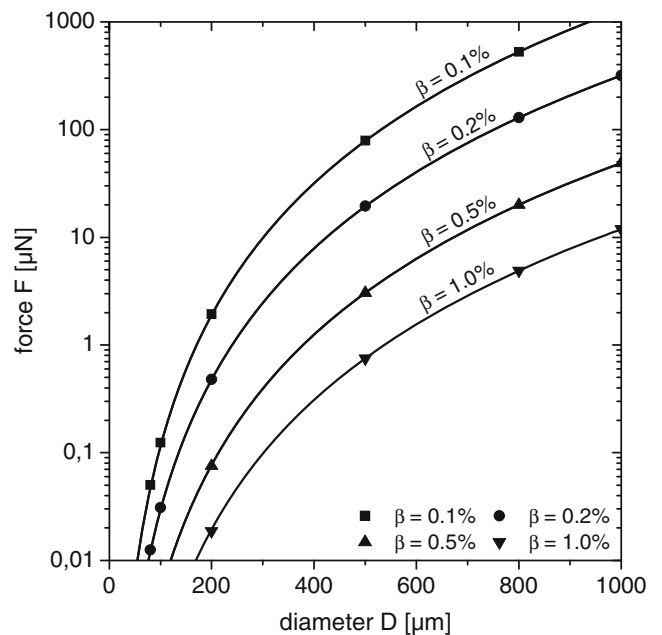
Fig. 4 Lines of constant approximation error $\beta = 1 - w/y$ in the force-diameter plane

Experimental realization

The (tilted) CaBER device

The tilted CaBER method has been realized by mounting a commercial CaBER-1 (Thermo Scientific, Karlsruhe) on a customized L-shaped aluminum construction in order to rotate the whole device by 90°, as shown in Fig. 3a. Thus, the liquid thread is stretched in horizontal direction and bents due to the action of gravity (Fig. 3b).

The device is equipped with plates of diameter $D_0 = 6$ mm. The liquid bridge is created by separating the plates from a displacement of $h_i = 0.51$ mm or $h_i = 0.75$ mm to a final displacement of $h_f = 6.5$ mm or $h_f = 11.5$ mm within a constant strike time of $t_s = 40$ ms.

The upper plate or, in case of the tilted experiment, the left plate reaches its final position at time $t_1 = t_0 + t_s$ where the filament diameter is referred to $D_1 = D(t_1)$. This notation considers the mismatch between time t_0 when the experiment starts and time t_1 when the capillary thinning begins. The thinning of the filament is recorded using a high-speed camera (Photron Fastcam-X 1024 PCI), a telecentric objective (MaxxVision TC4M 16, magnification: ×1) and a blue telecentric background light (Vision & Control, TZB30-B) as described by Niedzwiedz et al. (2009). The experimental setup allows observations within a resolution of 1,024 × 1,024 px (1 px ≈ 16 μm) and a frame rate of 1,000 fps. We assume that at least two pixels are needed for a reliable determination of the filament diameter, and we do not consider diameters lower than 32 μm. Each individual image is analyzed in order to determine the upper and lower edge of the filament. Here, we have taken care that edges are detected properly correct without any impaired results, which can occur due to pixel fault (too bright or dark pixel) of the camera or defective image recognition. Therefore, we have implemented an automatic procedure in MATLAB to examine each image individually relating to two aspects: the absolute value of the determined filament diameter must be lower than the diameter of the plates used and the maximum acceptable slope of the diameter is $(dD/dx)_{max} = 0.1$. All data points which do not satisfy these conditions are ignored in subsequent calculations.

Therewith, the experimental determined bending line or neutral axis (see also Fig. 3b) is calculated to apply Eqs. 19 and 20 for the force calculation The neutral axis is named W, this experimental value corresponds to the model value w in the case of the approximated theory and y in the case of the general theory. Regardless of the applicability of Eqs. 19 and

20, which will be discussed in more details below, the force calculation from the bending line (Eq. 20) requires a further treatment of the measured data. The insufficient horizontal adjustment of the CaBER device in a range of a few micrometers and a shear flow perpendicular to the axial filament direction (double arrows in Fig. 3b) in the contact areas between the fluid filament and the CaBER-plates (which can differ for each plate) induced a different position of filament for the left and the right edge in the tilted experiment. Therefore, we carried out a baseline correction for our data, which is based on the assumption of filament symmetry relative to the point of maximum deflection and contains the following strategy. We calculate the first derivative of the filament diameter dD/dx and determine the section where $dD/dx < 0.01$. The two discrete dD/dx values which are nearest to 0.01 are named L_1 for the left side and R_1 for the right side of the filament (Fig. 5a). These values define the borders for the baseline correction. Then the next five points in positive x-direction are considered, and the
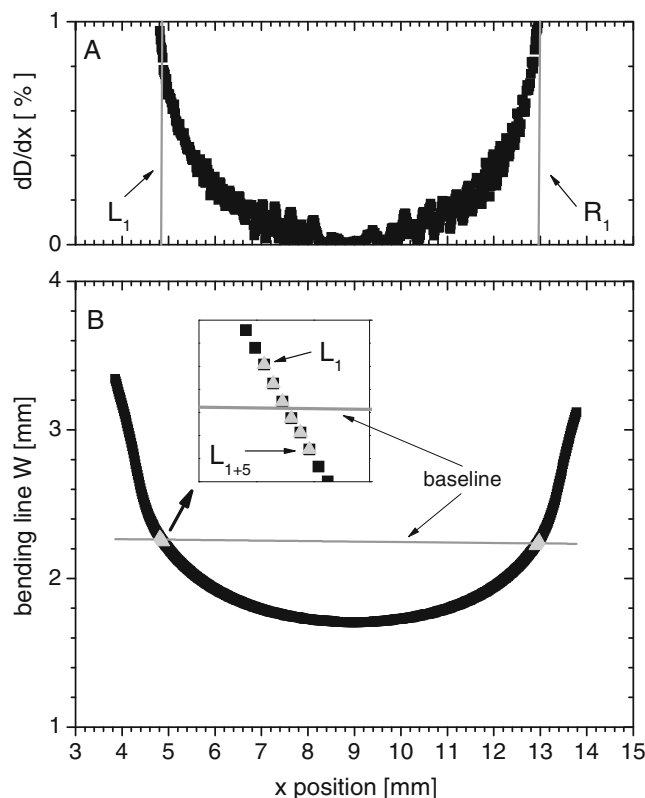
Fig. 5 **a** Derivation of the diameter with the determined left edge, L_1, and right edge, R_1. **b** Experimentally determined bending line W as a function of x-position. The *gray lines* represent the baseline BL calculated from L_1 to L_{1+5} and R_{1-5} to R_1 data points

average value $W_L = \sum_{i=0}^{5} W(L_{1+i})/6$ is calculated; then $W_R = \sum_{i=0}^{5} W(R_{1-i})/6$ is obtained analogously averaging over six points starting from $W(R_1)$ going into negative x-direction. Finally, the baseline BL is defined as the line connection of W_L and W_R (Fig. 5b). Then the corrected bending line W_{corr} is calculated according to $W_{corr} = W - BL$ and the lowest point of W_{corr} is chosen as point of reference so that $(W_{corr})_{min} = 0$ is guaranteed. Finally, the force is calculated applying Eq. 20. It has to be noted that the baseline correction has no visible influence for the force calculation based on Eq. 19.

Sample preparation and characterization

In this study, we used two different Newtonian model systems and one viscoelastic system. The first Newtonian system was composed of fructose (Carl Roth GmbH, Karlsruhe, Germany) solutions with mass fractions between 76 and 81 % in an aqueous mixture of 0.1 wt.% Tween20 (Carl Roth GmbH, Karlsruhe, Germany). The samples were stirred and heated for 3 h using a magnetic stirrer and were measured within 2 days to prevent recrystallization of the highly concentrated solutions (c ≥ 80 %). Zero shear viscosities η_0 were determined from steady state measurements using a MARS II rotational rheometer (Thermo Scientific) equipped with cone plate geometry

(60/35 mm in diameter and 1° cone angle) at 20 °C. The surface tension (measured with a platinum–iridium Wilhelmy-plate mounted on a DCAT 11, DataPhysics tensiometer) was constant for all samples within experimental error and was determined to $\Gamma \approx 62.8$ mN/m, which is approximately 20 mN/m lower than the surface tension of the pure aqueous fructose solutions. Therefore, the addition of surfactant has two effects: the filament lifetime of the fructose solutions is increased and the surface tension exhibits the same value as for the PEO solutions describe below. The second Newtonian system were mixtures of silicon oil AK50000 in AK1000 (both Wacker Chemie AG, Munich, Germany) with mass fractions between 0 and 100 %. Silicon oils are obviously non-Newtonian fluids, but they exhibit Newtonian flow behavior in CaBER experiments because the longest relaxation time λ_s is much smaller than the filament lifetime (compare Fig. 8 and data in Table 1). The elasto-capillary number Ec (Anna and McKinley 2001; Clasen 2010) provides a quantitative criterion to estimate this effect.

$$Ec = \frac{2\lambda_s \Gamma}{\eta_s D} \qquad (22)$$

It compares the viscous timescale $t_v = \eta_s D/2\Gamma$ with the timescale of elastically controlled thinning, assumed as the longest shear relaxation time λ_s which was

Table 1 Physical properties of the measured model systems

Type	c/%	$\eta_{s,0}$/Pa s	λ_s/ms	Γ/mN/m	ρ/g cm^{-3}	Ec_{max}
Fructose/Tween20	76.0	0.88 ± 0.01	–	61.8 ± 2.3	1.380	–
	77.0	1.19 ± 0.03	–	64.4 ± 1.9	1.385	–
	78.0	1.64 ± 0.08	–	62.2 ± 0.7	1.390	–
	79.2	2.47 ± 0.05	–	61.9 ± 0.3	1.398	–
	80.0	3.59 ± 0.07	–	62.0 ± 0.8	1.402	–
	81.0	5.00 ± 0.11	–	62.4 ± 0.6	1.420	–
AK50000	0	1.04 ± 0.01	0.19 ± 0.05	20.8 ± 0.5	0.972	0.2
	20	2.97 ± 0.01	0.82 ± 0.07			0.4
	40	8.11 ± 0.07	1.71 ± 0.03			0.3
	60	17.68 ± 0.23	3.26 ± 0.05			0.2
	80	34.11 ± 0.41	4.63 ± 0.12			0.2
	100	60.27 ± 1.18	5.97 ± 0.10			0.1
PEO 10^6 g/mol	1.0	0.04 ± 0.01	9.7 ± 1.3	61.7 ± 0.6	0.992	935
	1.5	0.14 ± 0.02	26 ± 2	62.7 ± 0.3	0.992	728
	2.0	0.38 ± 0.01	54 ± 3	61.7 ± 0.4	0.991	548
	2.5	0.94 ± 0.02	110 ± 8	62.8 ± 0.1	0.994	459
	3.0	2.01 ± 0.06	189 ± 8	62.8 ± 0.6	0.993	369
	3.5	4.10 ± 0.17	340 ± 15	62.5 ± 0.2	0.994	324
	4.0	8.58 ± 0.30	425 ± 21	62.8 ± 0.4	0.996	194
	4.5	12.97 ± 0.43	635 ± 27	61.0 ± 0.8	1.000	187
	5.0	25.46 ± 0.66	1005 ± 31	57.5 ± 0.5	1.005	142

determined by small amplitude oscillatory shear experiments according to

$$\lambda_s = \lim_{\omega \to 0} \frac{G'}{G''\omega} \tag{23}$$

using a Physica MCR 501 (Anton Paar) equipped with cone plate geometry (50-mm diameter and 1° cone angle) at 20 °C.

Elastically driven capillary thinning sets in when Ec ≈ 1. For the silicon oil mixtures investigated here, the maximum elasto-capillary number EC_{max} were calculated using the minimal observable diameter of $D_{min} = 32$ μm. In all cases investigated here, $Ec_{max} \ll 1$ was detected, corresponding data are summarized in Table 1.

Therefore, silicon oils are a useful Newtonian model system for CaBER experiments. The surface tension was only measured for pure AK1000 due to the high viscosity of the other samples, and we assumed a constant surface tension for all silicon oil mixtures.

PEO solutions with polymer mass fractions between 1 and 5 % were used as viscoelastic model system. The polymer powder (Aldrich Chemical Co., UK) had a weight average molecular weight of 10^6 g/mol and was dissolved in distilled water by means of shaking. The samples were stored at 7 °C up to the point of measurement. The surface tension of the PEO solutions is $\Gamma \approx 62.4$ mN/m and independent of polymer concentration up to c ≈ 4 %. A lower surface tension was observed for higher polymer concentration, probably due to systematic errors inferred from the high sample viscosity.

All data, including the density of the samples determined using a pycnometer with a total volume of 10.706 cm³ at 20 °C, are summarized in Table 1.

Results and discussion

Validation of the force calculation method

Figure 6 shows typical results of force calculation from gravity-driven bending of horizontally stretched fluid filaments as a function of diameter. The squares represent the 2.5 % PEO solution which behaves like a typical weakly viscoelastic fluid, indicated by a cylindrical thread in the CaBER experiment. The forces calculated using Eq. 20 (open symbols) and Eq. 19 (closed symbols) are identical within experimental uncertainty. Therefore, the simplified force calculation method, and particularly the parabolic fit of the bending line, yields good results as long as the thread is cylindrical.
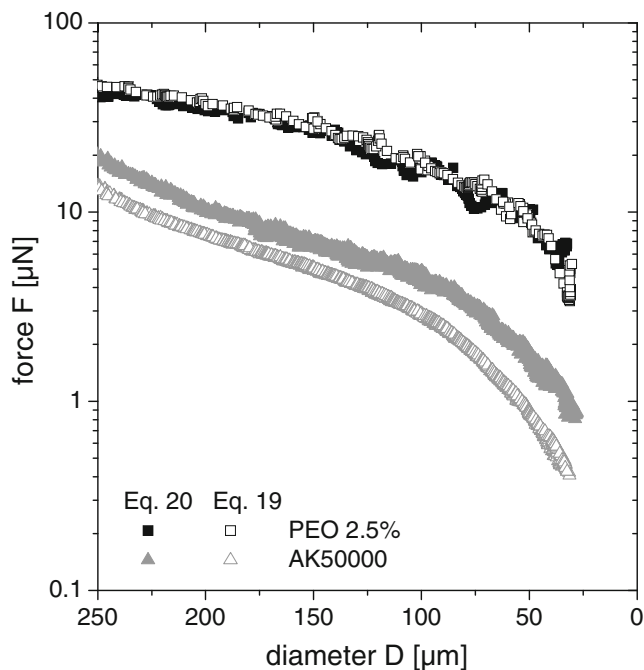

Fig. 6 Measured force F as a function of the diameter for the end of the filament thinning (measurement properties, $h_i = 0.51$ mm, $h_f = 11.5$ mm). *Closed symbols* represent data evaluation, using Eq. 20; and *open symbols* represent data evaluation, using Eq. 19, for a 2.5 % PEO solution (*squares*) and silicon oil AK50000 (*triangles*)

The Newtonian silicon oil AK50000 forms slightly concave filaments. The calculated forces (triangles in Fig. 6) differ from each other due to the non-constant diameter. The force values calculated using the numerical integration of the diameter (Eq. 20), represented by closed symbols, are significantly larger than the force values calculated by Eq. 19 with the assumption of constant diameter (open symbols). The corresponding Trouton ratios Tr defined as the ratio of the true elongational viscosity, calculated by applying Eq. 7, and the shear viscosity are Tr = 3.2 when the force is calculated according to Eq. 20 and Tr = 2.0 if Eq. 19 is applied. Of course, the correct Trouton ratio is three for a Newtonian fluid. This demonstrates that the filament curvature has to be taken into account for non-cylindrical filaments and as a consequence, we determine the force only by applying Eq. 20 for all cylindrical and non-cylindrical threads.

Figure 7 (left) shows the force ratio X as a function of diameter calculated directly from the force measurements according to Eq. F2 for three silicon oil mixtures. For all samples investigated here, X strongly decreases with decreasing diameter to a constant final value X_∞. This decrease is associated with the initial deflection of the liquid tread. The critical filament diameter, where X_∞ is reached, is shifted to lower
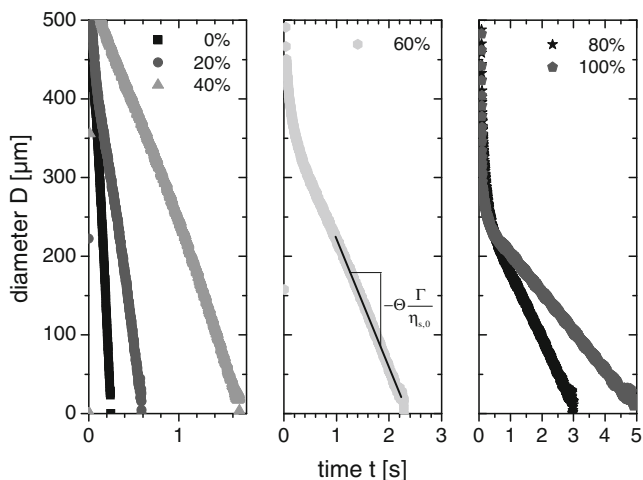
Fig. 7 *Left* Force ratio as a function of diameter for AK50000 in AK1000 mixture for three different concentrations given in the diagram. *Right* Image sequence of the deflection during the capillary breakup in the tilted CaBER experiment for the 20 % AK50000 mixture
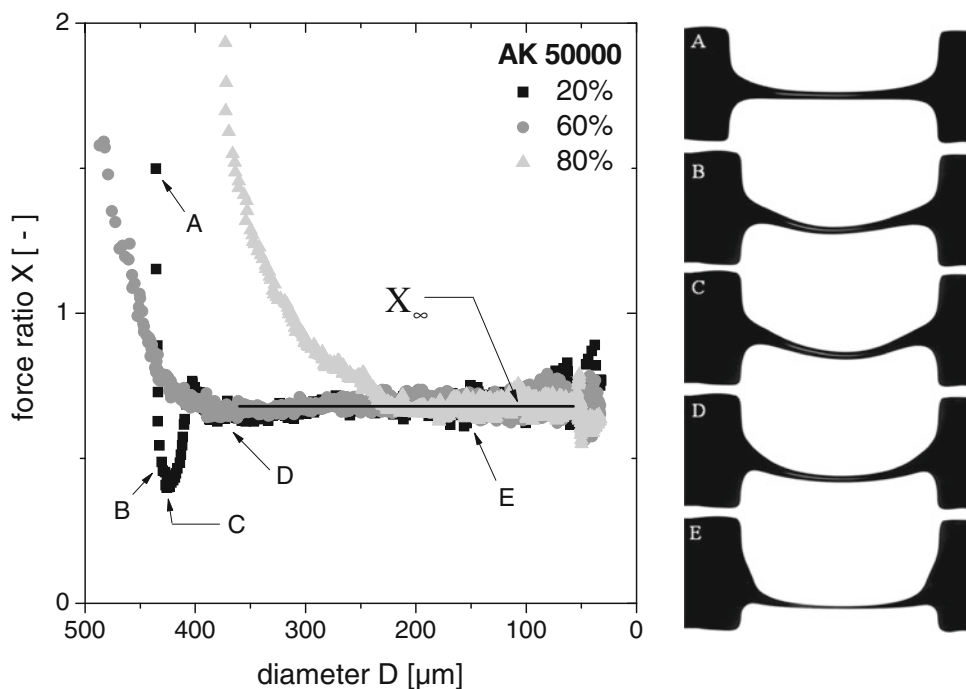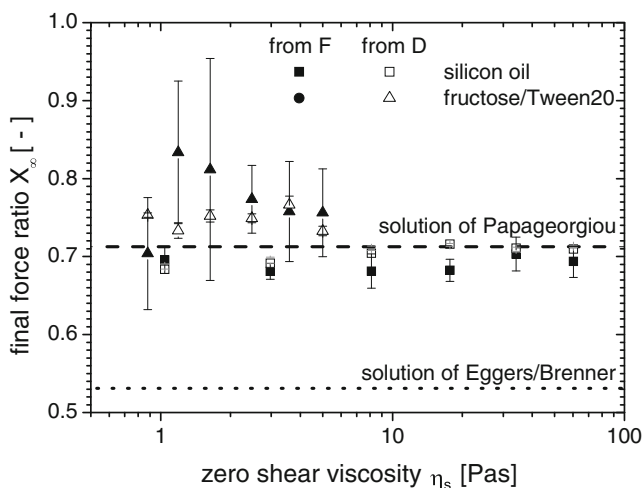
values with increasing AK50000 concentration and correspond to the inflection point of the filament diameter vs. time curves, shown in Fig. 8. The low viscous silicon oil mixture including of 20 % AK50000 additionally exhibits a sharp minimum before the constant X_∞ value is reached. This initial variation of X is attributed to a wave traveling through the filament after the plates have reached their final position. This wave results in a shift of the point of maximum deflection as shown in the images in Fig. 7. Image D where the filament deflection is symmetric corresponds to the diameter where X_∞ is reached. This finding is typical for low viscous Newtonian fluids with $\eta_s < 15$ Pa s. For the viscoelastic

Fig. 8 Diameter as a function of time for the AK50000 in AK1000 mixtures ($h_i = 0.51$ mm, $h_f = 11.5$ mm)

PEO solutions investigated here, a wave through the filament was only observed at a zero shear viscosity of $\eta_s = 0.04$ Pa s, corresponding to a concentration of 1.0 %. This phenomenon did not occur for solutions with higher PEO concentrations and this is attributed to the well-known stabilization effect of the stretched polymer coils (Lenczyk and Kiser 1971; Tirtaatmadja et al. 2006).

The consideration of the final force ratio allows for another way for the validation of the force calculation method. On one hand, X_∞ is determined directly from the force measurement as described above. On the other hand, X_∞ can also be calculated from the slope of $D(t)$ which is proportional to $-\Theta\Gamma/\eta_s$ (see Fig. 8), as expected for Newtonian fluids. Using Eq. 10 and the additionally measured zero shear viscosity, the numerical factor Θ is linked to the force ratio X_∞. Figure 9 shows the experimentally determined force ratios, as a function of viscosity for the two series of Newtonian fluids. Here, silicon oil mixtures (squares) were measured with an initial height of $h_i = 0.51$ mm and a final height of $h_f = 11.5$ mm and the fructose/Tween20 solutions (triangles) were measured with $h_i = 0.75$ mm and $h_f = 6.5$ mm. The large scale error bars of the fructose/Tween20 solutions are caused by the high capillary velocity Γ/η_s, and, hence, a short filament lifetime. The force ratio values determined from the diameter (open symbol) and the force (filled symbols) using Eq. 20 are identical within experimental error. Considering all force measurement experiments, we obtain an average force ratio $X_\infty = 0.728 \pm 0.059$, which is in

Fig. 9 Force ratio as a function of zero shear viscosity for silicon oil mixtures ($h_i = 0.51$ mm, $h_f = 11.5$ mm) and fructose/Tween20 solutions ($h_i = 0.75$ mm, $h_f = 6.5$ mm). The *filled symbols* represent X_∞ values using the calculated force, and the *open symbols* represent X_∞ values using the diameter

excellent agreement with the solution of Papageorgiou (1995) and which is far away from the solution of Eggers (1993, 1997) and Brenner et al. (1996). All these experiments validate the tilted CaBER method including the force calculation from Eq. 20 as an accurate and robust method for the determination of the axial force in a fluid filament during capillary thinning elongational flow.

Sign of the axial normal stress

From a theoretical point of view, the minimum $\sigma_{zz}/|\sigma_{rr}|$ value is -1 because lower values would result in negative elongational viscosities. Figure 10 shows the dimensionless normal stress ratio $\sigma_{zz}/|\sigma_{rr}|$ as a function of diameter for a silicon oil mixture of 60 % AK50000 in AK1000 (filled squares) and a 3.5 % PEO solution (open triangles).

During the initial thinning period dominated $\sigma_{zz}/|\sigma_{rr}|$ strongly decays in both cases. This decay is faster for fluids of lower viscosity and is presumably due to inertial effects. After this induction period $\sigma_{zz}/|\sigma_{rr}|$ reaches a constant value $\sigma_{zz}/|\sigma_{rr}| = -0.54 \pm 0.12$ for all Newtonian fluids. The negative sign corresponds to a compressive stress, which causes the pronounced deflections of Newtonian filaments. Such compressive stresses are not observed for the PEO solutions and, hence, the deflection is less pronounced compared to the Newtonian samples discussed in the previous section. The induction period is much shorter for all the investigated PEO solutions than for the silicon oils due to the damping properties of the polymer coils.
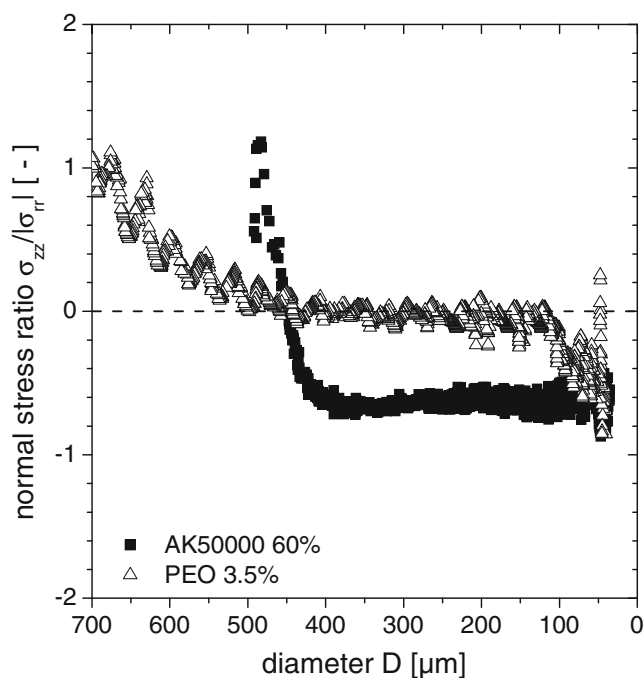
Fig. 10 Normal stress ratio for a 3.5 % PEO 10^6 g/mol solution (*filled squares*) and a 60 % AK50000 mixture (*open triangles*)

Accordingly, the asymptotic value for the normal stress ratio is reached much faster. A limiting value $\sigma_{zz}/|\sigma_{rr}| \approx 0$ is observed for the PEO solutions with concentrations lower than 4 %. For these sparsely concentrated solutions, it is not possible to check the assumption of Clasen et al. (2006a) that σ_{zz} increases exponentially due to the measuring accuracy and the scatter of the data points. Anyway, σ_{zz} must be significantly smaller than σ_{rr}, and in this case, the widely used assumption $\sigma_{zz} = 0$ obviously is valid for the evaluation of the elongational viscosity from CaBER measurements. But constant values $\sigma_{zz}/|\sigma_{rr}| > 0$ are observed for higher polymer concentrations as discussed in the next section. This finding is the experimental proof of significant exponentially increasing axial normal stresses as predicted by Clasen et al. (2006a).

$$\frac{\sigma_{zz}}{|\sigma_{rr}|} = \text{const.} \Rightarrow \sigma_{zz} \propto \frac{1}{D} \propto \exp\left(\frac{t}{3\lambda_e}\right) \qquad (24)$$

The normal stress ratio is related to the force ratio X discussed in the previous section. The force balance (Eqs. 1 and 3) yields:

$$\frac{\sigma_{zz}}{|\sigma_{rr}|} = 2\left(\frac{F}{\pi D \Gamma} - 1\right). \qquad (25)$$

Combining Eq. 25 with the definition of the force ratio (Eq. 2) results in

$$X = \frac{1}{2}\frac{\sigma_{zz}}{|\sigma_{rr}|} + 1. \qquad (26)$$

Therefore, the sign of σ_{zz} is obvious from the force ratio, as discussed above. For vanishing axial stresses, the force ratio is one. $X < 1$ values correspond to a compressive axial normal stress, and $X > 1$ values correspond to a tensile normal stress.

Applying the tilted CaBER method to non-Newtonian fluids

Recently, the behavior of semi-dilute and concentrated entangled PEO solutions in regular CaBER experiments has been discussed in detail (Arnolds et al. 2010). They obtained $c^* \approx 0.4\ \%$ and $c_e \approx 2.5\ \%$ for PEO with $M_w = 10^6$ g/mol from their steady and small amplitude oscillatory shear experiments. Here, we focus on the variation of the axial force in this concentration range investigating PEO solutions with concentrations between 1 and 5 %.

The filament lifetime of these PEO solutions strongly increases with polymer concentration. Diameter data are shown in Fig. 11a. The PEO solutions with $c < 4\ \%$ exhibit the typical exponential thinning (lines in Fig. 11a), with characteristic relaxation time λ_e, calculated according to Eq. F11. For higher polymer concentrations, the filaments are still cylindrical but do not exhibit an exponential thinning regime and, hence, λ_e cannot be determined. The findings are in good agreement with Arnolds et al. (2010). Corresponding force measurement data are shown in Fig. 11b. The force F decreases monotonically with time to a minimal value of about 1 μN.
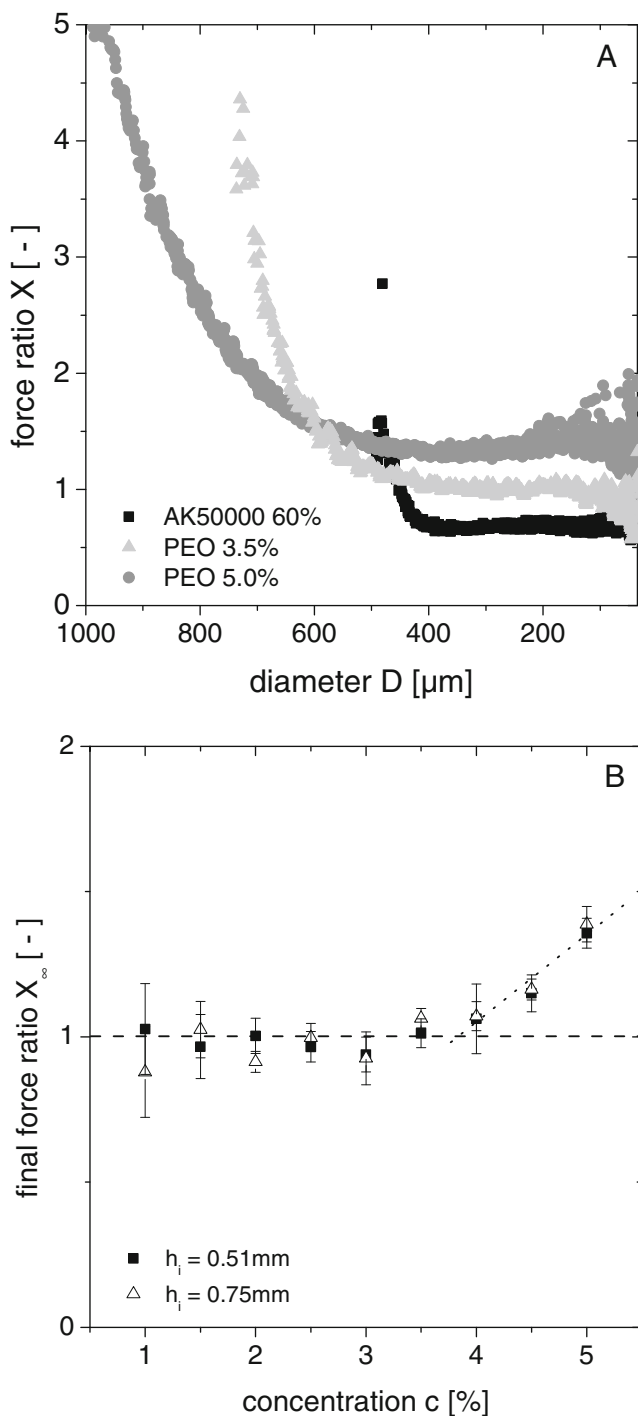
Calculated force ratios as a function of diameter D for PEO solutions with $c = 3.5\ \%$ and $c = 5.0\ \%$ as well as for the Newtonian silicon oil mixture AK50000 60 % are shown in Fig. 12a. The measured force ratios for the PEO solutions investigated here are always higher than the force ratio for the Newtonian liquid. Remarkably, this finding disagrees with the observation of Clasen (2010) for capillary breakup of semi-dilute polymer solutions. He observed that the thinning process splits up into four regimes: (1) early thinning which is controlled by gravitational sagging; (2) Newtonian thinning behavior (viscocapillary) described by Eq. 9; (3) extensional thinning (still viscocapillary) described by a power law; and finally (4) elasto-capillary thinning described by Eq. 11. It is clearly shown in Fig. 12a that the $X(D)$ data do not support the existence of Newtonian thinning regime because the Newtonian

limit of $X_\infty = 0.728 \pm 0.059$ is never reached during the thinning process. This emphasizes that the interpretation of the $D(t)$ data (Fig. 11a) as, e.g., done by Clasen (2010) is not unambiguous since the corresponding force ratio is not considered. Therefore, the force measurement gives additional information for the interpretation of the thinning behavior of liquid filaments.
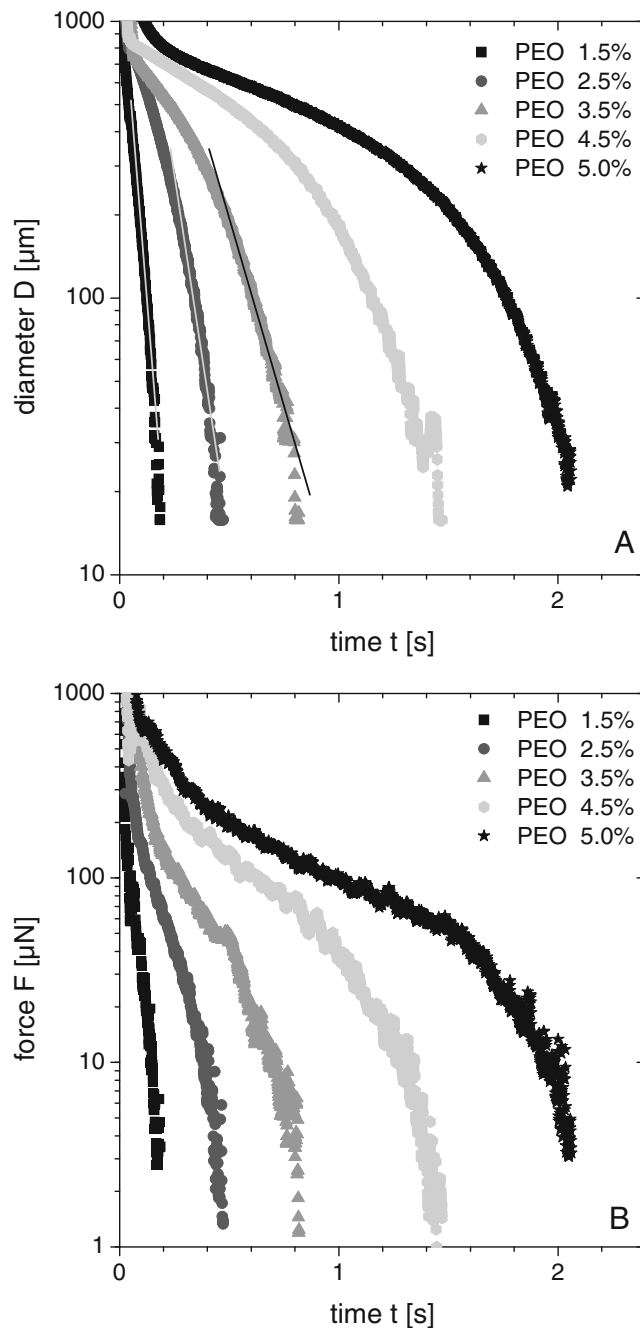
Fig. 11 PEO solutions CaBER measurements (measurement properties, $h_i = 0.51$ mm, $h_f = 11.5$ mm). **a** Diameter as a function of time. The *lines* represent exponential fits to the data. **b** Force as a function of time

The extracted final force ratios X_∞ versus concentration c for the investigated PEO solutions are shown in Fig. 12b. Remarkably, this ratio is one for the clearly elasto-capillary exponentially thinning solutions

Fig. 12 **a** Force ratio as a function of diameter. **b** Final force ratio as a function of concentration c for two different initial heights $h_i = 0.51$ mm (*filled squares*) and $h_i = 0.75$ mm (*open triangles*). The *dashed line* represents a vanishing axial normal stress

($c < 3.5$ %). $X_\infty = 1$ means that there is no axial stress in the filament during capillary thinning. Therefore, the simplified approach of calculating the elongational viscosity according to Eq. 8 is valid for these weakly elastic PEO solutions. However, the final force ratio deviates significantly from $X_\infty = 1$, indicating that $\sigma_{zz} \neq 0$ and increases monotonically for concentrations $c \geq 4$ %. Non-vanishing σ_{zz} values for non-Newtonian fluids are directly detected here for the first time performing CaBER experiments. This clearly indicates the limitations of the widely used, simplified data analysis for calculating the elongational viscosity (Eq. 8) and demonstrates that an accurate force measurement is mandatory for a determination of absolute η_e values (Eq. 7) from CaBER experiments.
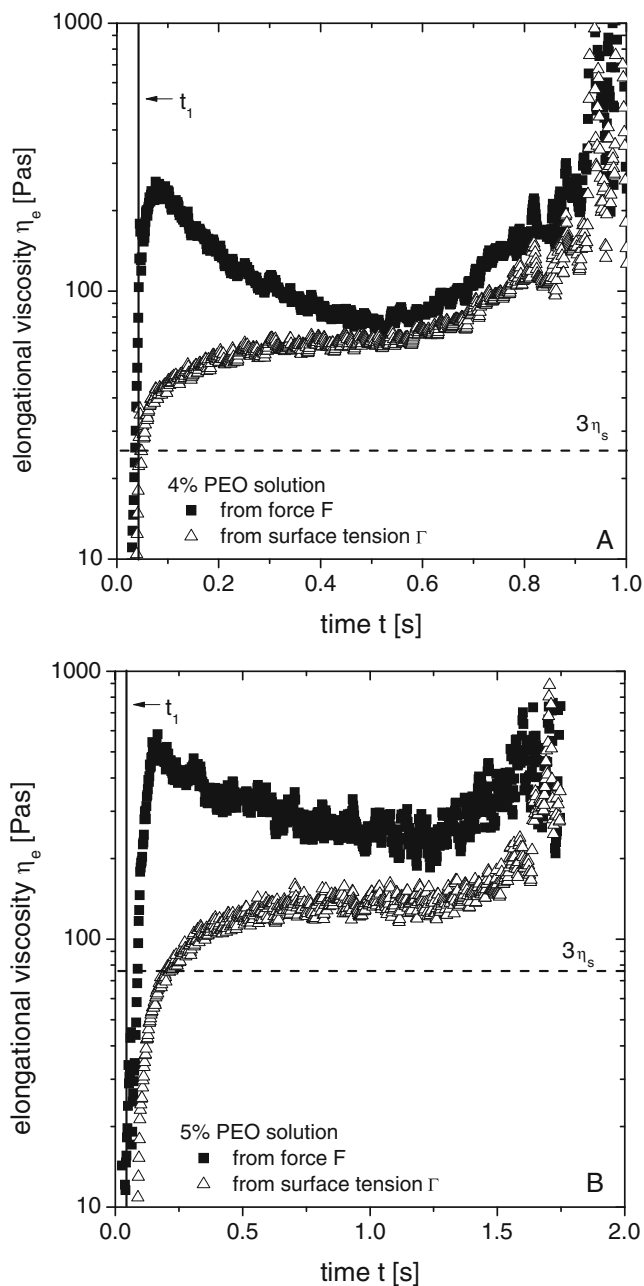
The concentration where X_∞ begins to differ from unity ($c = 4$ %) is much greater than the overlap concentration of c^* and roughly coincides with the entanglement concentration c_e. It seems that a significant axial normal stress is due to the entanglements present in these solutions and gives rise to the observed non-exponential thinning of the filament diameter.

In Fig. 13, the elongational viscosity η_e obtained from the force measurement is compared to the apparent elongational viscosity $\eta_{e,app}$ calculated from Γ and $D(t)$ using the $\sigma_{zz} = 0$ assumption for a 4.0 % PEO solution (Fig. 13a) and a 5.0 % PEO solution (Fig. 13b). Here, we have smoothed the diameter data applying the floating average method in order to calculate the elongation rate numerically.

In the initial period of capillary thinning right after the upper plate has reached its final position ($t > t_1$), the elongational viscosity η_e obtained from the force measurements goes through a sharp maximum, which does not appear in $\eta_{e,app}$. Similar results were obtained for all PEO solutions investigated here, but the apparent viscosity maximum is less pronounced for PEO solutions with higher polymer concentration.

The physical interpretation of this phenomenon is not yet clear, but it might be due to inertial effects as already discussed above (see "Validation of the force calculation method" and "Sign of the axial normal stress"). It also has to be noted that the elongation rate goes through a distinct minimum during this period of thinning. This topic requires further investigations which are beyond the scope of this paper.

The time when η_e reaches its minimum corresponds to the time when the force ratio X reaches its limiting value. For the PEO solutions with $c \leq 4$ %, the time also corresponds to the inset of the exponential thinning. In this case, the limiting value is independent of polymer concentration ($X_\infty = 1.1 \pm 0.1$). During the final stage of capillary thinning, both elongational vis-

Fig. 13 Elongational viscosity as a function of time (measurement parameters, $h_i = 0.75$ mm, $h_f = 11.5$ mm), calculated from force measurement data according to Eq. 7 (*filled squares*) and the surface tension (Eq. 8) assuming $\sigma_{zz} = 0$ (*open triangles*). **a** 4.0 % PEO solution. **b** 5.0 % PEO solution

significantly lower than the true value obtained from the force measurements.

Conclusions

We have introduced a new way of performing CaBER experiments named tilted CaBER method. This method comprises a horizontal stretching of fluid filaments and allows for a determination of the axial force in the liquid bridge from the gravity-driven bending of the filament applying chain bending theory. This method provides reliable values for the axial force in a liquid filament in a range of $N = 1,000$–0.1 μN and allows for a determination of the true elongational viscosity without additional assumptions or specific constitutive equations. For Newtonian fluids, the existence of a negative axial normal stress was proved experimentally, and the solution of Papageorgiou (1995) was confirmed for the linear thinning of Newtonian liquids by using two different sets of samples covering a viscosity range of $\eta_s = 0.9$–60 Pa s. The tilted CaBER method has been applied to non-Newtonian PEO solutions with concentrations $c > c^*$ and $c > c_e$. The assumption of vanishing axial normal stress for evaluating CaBER experiments was confirmed for solutions with $c < c_e$, and a positive axial normal stress was detected for concentrations above the entanglement concentration. In this case, the time evolution of the filament diameter no longer follows a simple exponential decay law. The elongational viscosity calculated from the measured force exhibits the well-known elongational hardening behavior also observed for other polymer solutions (Sridhar et al. 1991; Solomon and Muller 1996).

Appendix

Equation 7 for the calculation of the elongational viscosity in axial direction is only valid for slender filaments as investigated in this paper. Filament curvature must be taken into account in case of strongly non-cylindrical filaments which are typical for, e.g., yield stress fluids. At the position of the neck, the equilibrium condition in radial direction then reads as follows:

$$\sigma_{rr} = -\Gamma \left(\frac{2}{D_{mid}} - \frac{1}{|R_c|} \right) \tag{27}$$

cosity values η_e and $\eta_{e,app}$ strongly increase during the capillary thinning due to the well-known progressive entropic resistance to the deformation of the polymer chains; but in this case, $\eta_{e,app}$ is a reasonable approximation for the true elongational viscosity. For the 5 % PEO solution with $X_\infty > 1$, the apparent elongational viscosity during the final stage of thinning is

where D_{mid} is the diameter and R_c is the radius of curvature in axial direction at the neck. The expression for σ_{zz} does not change, and accordingly, the true elongational viscosity is given by

$$\eta_e = \frac{\sigma_{zz} - \sigma_{rr}}{\dot{\varepsilon}} = \frac{1}{dD_{mid}/dt}\left(\Gamma - \frac{2F}{\pi D_{mid}} + \frac{\Gamma D_{mid}}{2|R_c|}\right). \tag{28}$$

References

Agarwal S, Gupta RK (2002) An innovative extensional viscometer for low-viscosity and low-elasticity liquids. Rheol Acta 41:456–460

Alexandrou AN, Entov VM, Bazilevsky AV, Rozhkov AN, Sharaf A (2009) On the tensile testing of viscoplastic fluids. In: Acta rheological, special issue following the workshop: viscoplastic fluids: from theory to application, Nov. 1–5

Anna SL, McKinley GH (2001) Elasto-capillary thinning and breakup of model elastic liquids. J Rheol 45:115–138

Arnolds O, Buggisch H, Sachsenheimer D, Willenbacher N (2010) Capillary breakup extensional rheometry (CaBER) on semi-dilute and concentrated polyethylene oxide (PEO) solutions. Rheol Acta 49:1207–1217

Bazilevskii AV, Entov VM et al (1997) Failure of polymer solution filaments. Polym Sci A 39:316–324

Bazilevsky AV, Entov VM, Rozhkov AN (1990) Liquid filament microrheometer and some of its applications. In: Oliver DR (ed) Third European rheology conference. Elsevier, San Diego, pp 41–43

Bazilevsky AV, Entov VM, Rozhkov AN (2001) Breakup of an Oldroyd liquid bridge as a method for testing the rheological properties of polymer solutions. Polym Sci Ser A 43:716–726

Bhardwaj A, Miller E, Rothstein JP (2007) Filament stretching and capillary breakup extensional rheometry measurements of viscoelastic wormlike micelle solutions. J Rheol 51:693–719

Braun DB, Rosen MR (2000) Rheology modifiers handbook—practical use & application. William Andrew Publishing, Norwich, US

Brenner M, Lister J, Stone H (1996) Pinching threads, singularities and the number 0.0304. Phys Fluids 8:2827–2836

Chao KK, Child CA, Grens EA, Williams MC (1984) Antimisting action of polymeric additives in jet fuels. AIChE J 30:111–120

Christanti Y, Walker LM (2001a) Surface tension driven jet break up on strain-hardening solutions. J Non-Newton Fluid Mech 100:9–26

Christanti Y, Walker LM (2001b) Effect of fluid relaxation time of dilute polymer solutions on jet breakup due to a forced disturbance. J Rheol 46:733–748

Clasen C (2010) Capillary breakup extensional rheometry of semi-dilute polymer solutions. K-A Rheol J 22:331–338

Clasen C, Eggers J, Fontelos MA, Li J, McKinley GH (2006a) The beads on-string structure of viscoelastic threads. J Fluid Mech 556:283–308

Clasen C, Plog JP et al (2006b) How dilute are dilute solutions in extensional flows? J Rheol 50:849–881

Dexter RW (1996) Measurement of extensional viscosity of polymer solutions and its effects on atomization from a spray nozzle. At Sprays 6:167–191

Eggers J (1993) Universal pinching of 3D axisymmetric free-surface flows. Phys Rev Lett 71:3458–3490

Eggers J (1997) Nonlinear dynamics and breakup of free-surface flows. Rev Mod Phys 69:865–929

Entov VM, Hinch EJ (1997) Effect of a spectrum of relaxation times on the capillary thinning of a filament of elastic liquid. J Non-Newton Fluid Mech 72:31–53

Fernando RH, Lundberg DJ, Glass JE (1989) Importance of elongational flows in the performance of water-borne formulations. Adv Chem 223:245–259

Fernando RH, Xing LL, Glass JE (2000) Rheology parameters controlling spray atomization and roll misting behavior of waterborne coatings. Prog Org Coat 40:35–38

Gross D, Hauger W, Wriggers P (2009) Technische mechanik band 4: hydromechanik, elemente der höheren mechanik. Numerische Methoden Springer, Berlin

Han L, Gupta RK, Doraiswamy D, Palmer M (2004) Effect of liquid rheology on jetting of polymer solutions. In: XIVth int congr rheol, Seoul, KR

James DF, Yogachandran N, Roper JA III (2003) Fluid elasticity in extension, measured by a new technique, correlates with misting. In: 8th TAPPI advanced coating fundamentals symposium, Chicago, US, pp 166–171

Kennedy JC, Meadows J, Williams PA (1995) Shear and extensional viscosity characteristics of a series of hydrophobically associating polyelectrolytes. J Chem Soc Faraday Trans 91:911–916

Kheirandish S, Gubaydullin I, Willenbacher N (2008) Shear and elongational flow behaviour of acrylic thickener solutions, Part I: effect of intermolecular aggregation. Rheol Acta 49:397–407

Klein CO, Naue IF et al (2009) Addition of the force measurement capability to a commercially available extensional rheometer (CaBER). Soft Mater 7:242–257

Kolte MI, Szabo P (1999) Capillary thinning of polymeric filaments. J Rheol 43:609–626

Lenczyk JP, Kiser KM (1971) Stability of vertical jets of non-Newtonian fluids. AIChE J 17:826–831

Liang RF, Mackley MR (1994) Rheological characterization of the time and strain dependence for polyisobutylene solutions. J Non-Newton Fluid Mech 52:387–405

McKay GR, Ferguson J, Hudson NE (1978) Elongational flow and the wet spinning process. J Non-Newton Fluid Mech 4:89–98

McKinley GH, Tripathi A (2000) How to extract the Newtonian viscosity from capillary breakup measurements in a filament rheometer. J Rheol 44(3):653–670

Meadows J, Williams PA, Kennedy JC (1995) Comparison of extensional and shear viscosity characteristics of aqueous hydroxyethyl cellulose solutions. Macromol 28:2683–2692

Ng SL, Mun RP, Boger DV, James DF (1996) Extensional viscosity measurements of dilute solutions of various polymers. J Non-Newton Fluid Mech 65:291–298

Niedzwiedz K, Arnolds O, Willenbacher N, Brummer R (2009) How to characterize yield stress fluids with capillary breakup extensional rheometry (CaBER)? Appl Rheol 19:41969–1–41969–10

Oliveira MSN, Yeh R, McKinley GH (2006) Iterated stretching, extensional rheology and formation of beads-on-string structures in polymer solutions. J Non-Newton Fluid Mech 137:137–148

Papageorgiou DT (1995) On the breakup of viscous liquids threads. Phys Fluids 7:1529–1544

Plog JP, Kulicke WM, Clasen C (2005) Influence of the molar mass distribution on the elongational behaviour of polymer solutions in capillary breakup. Appl Rheol 15:28–37

Prud'homme RK, Smith-Romanogli V, Dexter RW (2005) Elongational viscosity effects in spraying processes. In: 230th ACS national meeting, Washington, US

Schümmer P, Tebel KH (1983) A new elongational rheometer for polymer solutions. J Non-Newton Fluid Mech 12(3): 331–347

Solomon MJ, Muller SJ (1996) The transient extensional behavior of polystyrene-based Boger fluids of varying solvent quality and molecular weight. J Rheol 40:837–856

Sridhar T, Tirtaatmadja V, Nguyen DA, Gupta RK (1991) Measurement of extensional viscosity of polymer solutions. J Non-Newton Fluid Mech 40(3):271–280

Stelter M, Brenn G, Yarin AL, Singh RP, Durst F (2002) Investigation of the elongational behavior of polymer solutions by means of an elongational rheometer. J Rheol 46:507–527

Tan H, Tam KC, Tirtaatmadja V, Jenkins RD, Bassett DR (2000) Extensional properties of model hydrophobically modified alkali-soluble associative (HASE) polymer solutions. J Non-Newton Fluid Mech 92:167–185

Tirtaatmadja V, McKinley GH, Cooper-White JJ (2006) Drop formation and breakup of low viscosity elastic fluids: effects of molecular weight and concentration. Phys Fluids 18:043101

Vadillo DC et al (2010) Evaluation of ink jet fluid's performance using the "Cambridge Trimaster" filament stretch and breakup-device. J Rheol 54(2):261–282

Webster MF, Matallah et al (2008) Numerical modeling of Stepp-strain for stretched filaments. J Non-Newton Fluid Mech 151:38–58

Willenbacher N, Matter Y, Gubaydullin I (2008) Effect of aggregation on shear and elongational flow properties of acrylic thickeners. K-A Rheol J 20:109–116